Mamy & Gaultier (1976). The *hk* lines are no longer straight, but have the shapes described by Bernal (1926) for rotation photographs. It is difficult, however, to prepare good specimens. Other arrangements have been developed recently with advantages for precise intensity measurements. The reflections are recorded consecutively by means of a powder diffractometer fitted with a goniometer head. The relation between the angle of tilt φ and the angle of diffraction (twice the Bragg angle) 2θ depends on the reciprocal-lattice point to be recorded. If the latter is defined by a vector of length $H = (2\sin\theta)/\lambda$ and by the angle ω between the vector and the plane of orientation (texture basis), the relation $\varphi = \theta - \omega$ permits scanning of reciprocal space along any trajectory by proper choice of consecutive values of ω or θ. In particular, if ω is constant, the trajectory is a straight line passing through the origin at an angle ω to the plane of orientation (Krinary, 1975). Using additional conditions [$\omega = \arctan(D/B)$, $H = (B^2 + D^2)^{1/2}$], Plançon *et al.* (1982) realized the recording and the measurement of intensities along the cylinder-generating *hk* rods for different shapes of the misorientation function $N(\alpha)$.

In the course of development of electron diffractometry, a deflecting system has been developed that permits scanning the electron diffraction pattern across the fixed detector along any direction over any interval (Fig. 4.3.5.2). The intensities are measured point by point in steps of variable length. This system is applicable to any kind of two-dimensional intensity pattern, and in particular to texture patterns (Zvyagin, Zhukhlistov & Plotnikev, 1996). Electron diffractometry provides very precise intensity measurements and very reliable structural data (Zhukhlistov *et al.*, 1997).

If the effective thickness of the lamellae is very small, of the order of the lattice parameter c, the diffraction pattern generates into a combination of broad but recognizably distinct $00l$ reflections and broad asymmetrical *hk* bands (Warren, 1941). The classical treatments of the shape of the bands were given by Méring (1949) and Wilson (1949) [for an elementary introduction see Wilson (1962)].

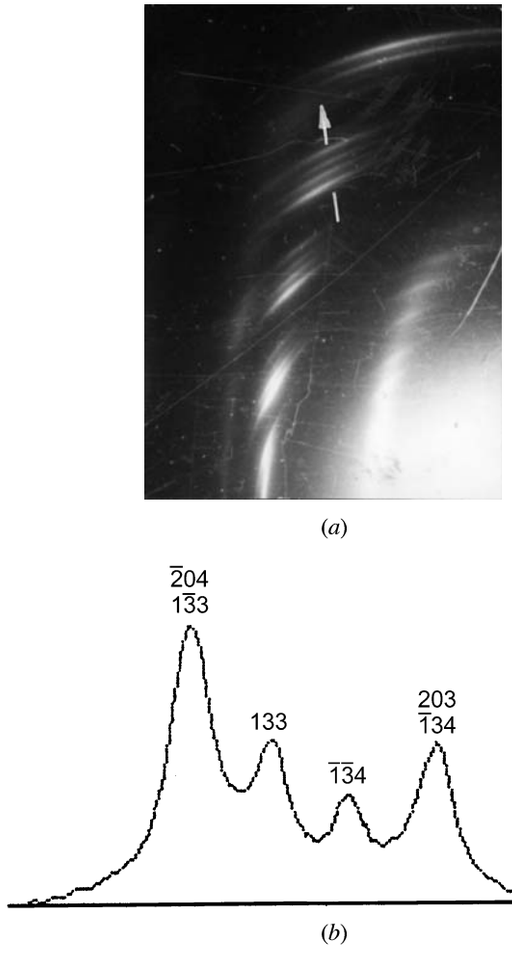

Fig. 4.3.5.2. (*a*) Part of the OTED pattern of the clay mineral kaolinite and (*b*) the intensity profile of a characteristic quadruplet of reflections recorded with the electron diffractometry system. The scanning direction is indicated in (*a*).

4.3.5.3. *Lattice direction oriented parallel to a direction (fibre texture)*

A fibre texture occurs when the crystals forming the specimen have a single direction in common. Each point of the reciprocal lattice describes a circle lying in a plane normal to the texture axis. The pattern, considered as plane sections of the reciprocal-lattice representation, resembles rotation diagrams of single crystals and approximates to the patterns given by cylindrical lattices (characteristic, for example, of tubular crystals).

If the *a* axis is the texture axis, the *hk* rods are at distances

$$B_{hk} = (-h\cos\gamma/a + k/b)/\sin\gamma \qquad (4.3.5.8)$$

from the texture axis and

$$D_{hk} = h/a \qquad (4.3.5.9)$$

from the plane normal to the texture axis (the zero plane b^*c^*). On rotation, they intersect the plane normal to the incident beam and pass through the texture axis in layer lines at distances D_{hk} from the zero line, while the reflection positions along these lines are defined by their distances from the textures axis (see Fig. 4.3.5.3):

$$B_{hkl} = [B_{hk}^2 + (-hx_n - ky_n + l)^2/d_{001}^2]^{1/2}. \qquad (4.3.5.10)$$

If the texture axis forms an angle ε with the *a* axis and $\delta = \varepsilon - \gamma + \pi/2$ with the projection of a^* on the plane *ab*, then

$$B_{hk} = \{-h(\sin\delta)/a + k[\sin(\gamma' - \delta)]/b\}/\sin\gamma \qquad (4.3.5.11)$$

$$= \{-h[\cos(\gamma - \varepsilon)]/a + k\cos\varepsilon/b\}/\sin\gamma \qquad (4.3.5.12)$$

$$D_{hk} = \{h(\cos\delta)/a + k[\cos(\gamma' - \delta)]/b\}/\sin\gamma \qquad (4.3.5.13)$$

$$= \{h[\sin(\gamma - \varepsilon)]/a + k\sin\varepsilon/b\}/\sin\gamma. \qquad (4.3.5.14)$$

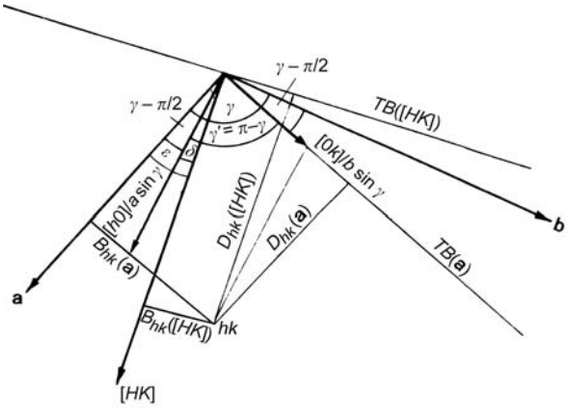

Fig. 4.3.5.3. The projections of the reciprocal axes on the plane *ab* of the direct lattice, with indications of the distances *B* and *D* of the *hk* rows from the fibre-texture axes *a* or [*hk*].

The relation between the angles δ, ε, and the direction $[hk]$ of the texture axis is given by the expression

$$\begin{aligned}\cos\delta &= \sin(\gamma-\varepsilon)\\ &= [h/a - k(\cos\gamma)/b]\\ &\quad\times [h^2a^{-2} + k^2b^{-2} - 2hk(\cos\gamma)/ab]^{-1/2}. \qquad (4.3.5.15)\end{aligned}$$

The layer lines with constant h that coincide when $\varepsilon = 0$ are split when $\varepsilon \neq 0$ according to the sign of k, since then $D_{hk} \neq D_{h\bar{k}}$ and B_{hk} and B_{hkl} defining the reflection positions along the layer line take other values. Such peculiarities have been observed by means of selected-area electron diffraction for tabular particles and linear crystal aggregates of some phyllosilicates in the simple case of $\gamma = \pi/2$ (Gritsaenko, Zvyagin, Boyarskaya, Gorshkov, Samotoin & Frolova, 1969).

When fibres or linear aggregates are deposited on a film (for example, in specimens for high-resolution electron diffraction) with one direction parallel to a plane, they form a texture that is intermediate between lamellar and fibre. The points of the reciprocal lattice are subject to two rotations: around the fibre axis and around the normal to the plane. The first rotation results in circles, the second in spherical bands of different widths, depending on the position of the initial point relative to the texture axis and the zero plane normal to it. The diffraction patterns correspond to oblique plane sections of reciprocal space, and consist of arcs having intensity maxima near their ends; in some cases, the arcs close to form complete circles. In particular, when the particle elongation is in the a direction, the angular range of the arcs decreases with h and increases with k (Zvyagin, 1967).

4.3.5.4. *Applications to metals and organic materials*

The above treatment, though general, had layer silicates primarily in view. Texture studies are particularly important for metal specimens that have been subjected to cold work or other treatments; the phenomena and their interpretation occupy several chapters of the book by Barrett & Massalski (1980). Similarly, Kakudo & Kasai (1972) devote much space to texture in polymer specimens, and Guinier (1956) gives a good treatment of the whole subject. The mathematical methods for describing and analysing textures of all types have been described by Bunge (1982; the German edition of 1969 was revised in many places and a few errors were corrected for the English translation).

4.3.6. Computation of dynamical wave amplitudes

4.3.6.1. *The multislice method (By D. F. Lynch)*

The calculation of very large numbers of diffracted orders, *i.e.* more than 100 and often several thousand, requires the multislice procedure. This occurs because, for N diffracted orders, the multislice procedure involves the manipulation of arrays of size N, whereas the scattering matrix or the eigenvalue procedures involve manipulation of arrays of size N by N.

The simplest form of the multislice procedure presumes that the specimen is a parallel-sided plate. The surface normal is usually taken to be the z axis and the crystal structure axes are often chosen or transformed such that the c axis is parallel to z and the a and b axes are in the xy plane. This can often lead to rather unconventional choices for the unit-cell parameters. The maximum tilt of the incident beam from the surface normal is restricted to be of the order of 0.1 rad. For the calculation of wave amplitudes for larger tilts, the structure must be reprojected down an axis close to the incident-beam direction. For simple calculations, other crystal shapes are generally treated by the column approximation, that is the crystal is presumed to consist of columns parallel to the z axis, each column of different height and tilt in order to approximate the desired shape and variation of orientation.

The numerical procedure involves calculation of the transmission function through a thin slice, calculation of the vacuum propagation between centres of neighbouring slices, followed by evaluation in a computer of the iterated equation

$$u_n(h,k) = p_n\{p_{n-1}\ldots p_3[p_2(p_1q_1 * q_2) * q_3] * \ldots * q_n\} \quad (4.3.6.1)$$

in order to obtain the scattered wavefunction, $u_n(h,k)$, emitted from slice n, *i.e.* for crystal thickness $H = \Delta z_1 + \Delta z_2 + \ldots + \Delta z_n$; the symbol $*$ indicates the operation 'convolution' defined by

$$f_1(x) * f_2(x) = \int_{-\infty}^{\infty} f_1(w) f_2(x-w)\,\mathrm{d}w,$$

and

$$p_n = \exp\left(-i2\pi\Delta z_n(\lambda/2)\{[h(h-h'')/a^2] + [k(k-k'')/b^2]\}\right)$$

is the propagation function in the small-angle approximation between slice $n-1$ and slice n over the slice spacing Δz_n. For simplicity, the equation is given for orthogonal axes and h'', k'' are the usually non-integral intercepts of the Laue circle on the reciprocal-space axes in units of $(1/a)$, $(1/b)$. The excitation errors, $\zeta(h,k)$, can be evaluated using

$$\zeta(h,k) = -(\lambda/2)\{[h(h-h'')/a^2] + [k(k-k'')/b^2]\}. \qquad (4.3.6.2)$$

The transmission function for slice n is

$$q_n(h,k) = F\{\exp[i\sigma\varphi_n(x,y)\Delta z_n]\}, \qquad (4.3.6.3)$$

where F denotes Fourier transformation from real to reciprocal space, and

$$\varphi_n(x,y)\Delta z_n = {}^p\varphi(x,y) = \int_{z_{n-1}}^{z_{n-1}+\Delta z_n} \varphi(x,y,z)\,\mathrm{d}z$$

and

$$\sigma = \frac{\pi}{W\lambda}\,\frac{2}{1+(1-\beta^2)^{1/2}}$$

and

$$\beta = \frac{v}{c},$$

where W is the beam voltage, v is the relativistic velocity of the electron, c is the velocity of light, and λ is the relativistic wavelength of the electron.

The operation $*$ in (4.3.6.1) is most effectively carried out for large N by the use of the convolution theorem of Fourier transformations. This efficiency presumes that there is available an efficient fast-Fourier-transform subroutine that is suitable for crystallographic computing, that is, that contains the usual crystallographic normalization factors and that can deal with a range of values for h, k that go from negative to positive. Then,

$$u_n(h,k) = F\{F^{-1}[u_{n-1}(h,k)]F^{-1}[q_n(h,k)]\}, \qquad (4.3.6.4)$$

where F denotes

$$u(h,k) = \frac{1}{n_x n_y}\sum_{x=1}^{n_x}\sum_{y=1}^{n_y} U(x,y)\exp\left\{2\pi i\left[\frac{hx}{n_x},\frac{ky}{n_y}\right]\right\}$$

and F^{-1} denotes

references